Accurate, Precise, and Verifiable Photoluminescence Efficiency of
Colloidal Quantum Dots Sols by Photothermal Threshold Quantum Yield Analysis
Peer-reviewed author version

# Accurate, Precise and Verifiable, Photoluminescence Efficiency of Colloidal Quantum Dots Sols by Photothermal Threshold Quantum Yield Analysis

Pieter Schiettecatte,[†,‡,§] Sigurd Mertens,[¶,§] Luca Giordano,[†,‡] Koen Vandewal,[*,¶]

and Zeger Hens[*,†,‡]

†Physics and Chemistry of Nanostructures, Department of Chemistry, Ghent University,
B-9000 Gent, Belgium

‡Center for Nano- and Biophotonics, Ghent University, B-9052 Gent, Belgium

¶IMO-IMOMEC, and Institute for Materials Research, Hasselt University, Wetenschapspark
1, 3590 Diepenbeek, Belgium

§Contributed equally to this work

E-mail: koen.vandewal@uhasselt.be; zeger.hens@ugent.be

## Abstract

Colloidal quantum dots (QDs) have become multi-purpose luminophores that combine a broad excitation with a narrow emission spectrum. Applications in displays, lighting, or solar-energy conversion, however, require quantum dots that have a photoluminescent quantum yield (PLQY) approaching unity. This need makes the accurate, precise and verifiable determination of the photoluminescence efficiency of QDs of utmost importance for the field. Here, we describe photothermal threshold quantum

yield as a calorimetric method for measuring the PLQY of QDs in liquid dispersions. Taking the example of InP-based core/shell QDs, we detail the principles behind the analysis, and we benchmark results relative to the spectroscopic determination using an absolute PLQY measurement with an integrating sphere. We argue that the accuracy of the method for highly efficient emitters, and the simplicity of the data and the data analysis make photothermal threshold quantum yield well suited for certifying the photoluminescence efficiency of QDs.

# Introduction

Colloidal quantum dots (QDs) have size-tunable optical properties characterized by a broad absorption and a narrow emission spectrum, and are suitable for solution-based processing.[1] This combination makes QDs a printable semiconductor that has been used as light absorber in solar cells and infrared sensors,[2,3] or as light emitter in displays,[4,5] lighting,[6,7] and luminescent solar concentrators.[8] In these applications, light emission by QDs most often involves the conversion of short-wavelength absorbed light into long-wavelength emitted light by photoluminescence. However, to make devices using such a photon downconversion step feasible, QDs are needed with a photoluminescence quantum yield (PLQY) that approaches unity. Otherwise, self-absorption will prevent photoluminescent light from reaching the edges of a luminescent solar concentrator,[9] or cause excessive heating that compromises the operation of light emitting diodes using QDs as the color convertor.[7] Promoting radiative recombination of photo-excited QDs has been accomplished by passivating localized states at the QD surface that act as centers for charge-carrier trapping, either by the judicious adaptation of the surface-terminating moieties,[10] or the epitaxial overgrowth of a core QD by a wide band gap shell.[11–13] As a result, a near-unity PLQY has been reported for numerous QD systems, such as CdTe and $CsPbCl_3$ core QDs,[14,15] or CdSe/CdS core/shell and InP/ZnSe/ZnS core/shell/shell QDs.[16–18]

When indeed PLQY is essential for the operation of QD devices using luminescent color

conversion, the reported PLQY ($\Phi_{PL}$) for a QD batch resulting from a given synthetic protocol should be accurate, precise and verifiable. Taking literature reports on highly efficient InP-based QDs as an example,[17–25] studies typically provide $\Phi_{PL,IS}$, i.e., an estimate of $\Phi_{PL}$ obtained by quantifying light absorption and emission by means of an integrating sphere.[26] While the standard deviation on an estimated $\Phi_{PL,IS}$ can be as low as $\pm 0.1\%$ when multiple measurements are analysed,[27] most studies use data from single measurements, which rather have an accuracy of $\pm 5\%$.[28] Moreover, any $\Phi_{PL,IS}$ calculated from measured spectra depends on the detector calibration and on the measurement protocol, which includes fine details ranging from slit settings to ensuring detector linearity. Few studies, if any, report the underlying data and analysis protocols. Hence, errors on reported values can be considerably larger than $\pm 5\%$, and data quality is difficult to assess.

In contrast with spectroscopic approaches, which aims at quantifying all absorbed and emitted photons, calorimetric methods derive $\Phi_{PL}$ from the comparison between the dissipation rate of thermal energy due to non-radiative recombination of photo-excited luminophores and the power absorbed by the luminophores. However, methods that directly measure the absorbed power, for example through the analysis of thermal gratings or thermal lenses, still require reference measurements on non-luminescent samples or knowledge about the thermal properties of the investigated samples.[29,30] This complication can be avoided when measuring the heat generated per absorbed photon, albeit in relative units, as a function of the excitation photon energy. Such a measurement can be achieved by combining, in a single setup, a photothermal deflection spectrometer with an absorption,[31] or a photoluminescence spectrometer.[32,33] In this so-called photothermal threshold quantum yield (PTQY) approach, proper calibration of the measurement setup results in a linear relation between the relative thermal loss per excitation ($\varepsilon_{TL}$) and the photon energy of excitation ($\varepsilon_{exc}$). Despite using relative units, such a heat-per-excitation curve not only enables $\Phi_{PL}$ to be calculated by extrapolation to the zero-loss photon energy, but also provides a dataset that can be readily conveyed and interpreted. Recently, PTQY was applied to thin films of polymer-embedded

3

CdSe/CdS QDs,[32] showing the capability of the approach to measure a PLQY of 99.6% with an 0.2% error. Given the need for accurate and verifiable PLQY measurements in QD research, it thus appears that the field may profit from the widespread use of PTQY to quantify the PLQY, either for the direct analysis of QD samples or the external calibration of the widely used integrating sphere setups for PLQY determination.

In this Protocols and Methods paper, we detail a protocol for applying PTQY to quantify the PLQY of colloidal QD sols, a stage of sample processing that is closer to the immediate product of a QD synthesis than QD-in-polymer films. We first describe PTQY as an experimental method to quantify the PLQY of QDs, providing details on the PTQY concept, the measurement setup and protocol, and the data analysis. Next, we use the example of red-emitting InP-based colloidal QDs to illustrate the technique, and make a comparison between $\Phi_{\text{PL,PT}}$ and $\Phi_{\text{PL,IS}}$, i.e., the PLQY obtained through PTQY and through spectroscopic analysis by means of an integrating sphere, respectively. We show that linear heat-per-excitation curves are obtained for samples with a $\Phi_{\text{PL,IS}}$ ranging between 61 and 99%, and that $\Phi_{\text{PL,PT}}$ agrees, within the margin of error, with these numbers. Based on these results, we argue that PTQY could be used as a method of choice for certifying the PLQY of a given QD batch, or verifying PLQY quantification protocols implemented on an integrating sphere setup.
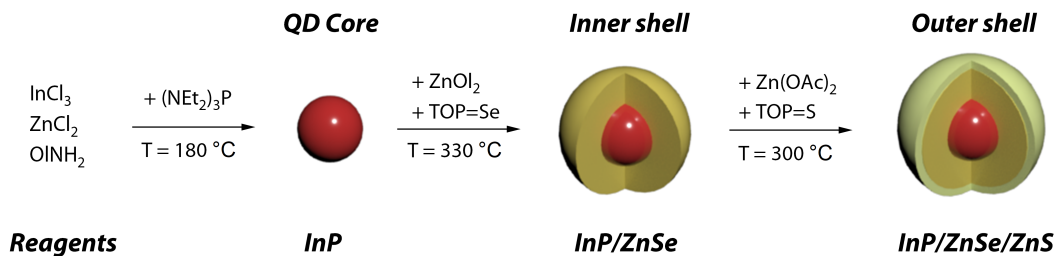


Figure 1: Schematic representation of synthesis of InP/ZnSe/ZnS core/shell quantum dots.

# Materials and Methods

## Colloidal InP-Based Core/Shell Quantum Dots

We produced a set of six different InP/ZnSe and InP/ZnSe/ZnS core/shell QDs using a previously published method.[18] As depicted in **Figure 1**, InP core QDs were grown in oleylamine ($OlNH_2$) at elevated temperatures by reacting tris(diethyl)aminophosphine ($P(NEt_2)_3$) with indium chloride ($InCl_3$) in the presence of zinc chloride ($ZnCl_2$).[34] Subsequently, the InP cores were overcoated with a ZnSe inner shell using tri-$n$-octylphosphine selenide (TOP=Se) and zinc oleate ($Zn(OA)_2$) as reactants. Next, an outer ZnS shell was grown around the InP/ZnSe QDs by reacting zinc acetate ($Zn(Ac)_2$) with tri-$n$-octylphosphine sulfide (TOP=S).[18] Detailed synthesis protocols and experimental conditions can be found in the **Supporting Information Section S1**. Samples A to D are state-of-the-art near-unity PLQY InP/ZnSe/ZnS QDs, while samples E and F are InP/ZnSe QDs with a lower PLQY.

## Photoluminescent Quantum Yield Measurement Using an Integrating Sphere

We used a standard two-measurement approach to determine $\Phi_{PL,IS}$, placing either the sample or a blank in the path of the incident beam.[35] All measurements have been run on an Edinburgh Instruments FLSP920 / FSP920 spectrometer using a 450 W Xenon lamp as steady state excitation source and a Hamamatsu R928P PMT as detector. For these PLQY measurements, the QD sols were diluted in anhydrous toluene in a nitrogen-filled glove box to obtain an optical absorbance of 0.1 to 0.2 at the excitation wavelength. The QD sols were photo-excited at 420 nm using an excitation slit of 4 nm, while the photoluminescence was analysed by means of an emission slit of 0.2 nm. In the spectral region between 400 and 440 nm, the spectrum was scanned in steps of 0.2 nm to accurately retrieve the 420 nm excitation band, while the spectral range between 440 and 750 nm was scanned in steps of 1 nm to measure the QD PL. Identical measurements were performed on a blank containing only

the solvent. We used the software of the FS900 Edinburgh Instruments spectrometer setup to retrieve $\Phi_{\text{PL,IS}}$. A more elaborate description of this procedure is given in **Supporting Information Section S2**.

## Photothermal Threshold Quantum Yield

For PTQY measurements, the QD sols were diluted in anhydrous toluene in a nitrogen-filled glove box. The liquid dispersion was placed in a quartz cuvette with a path length of 3 mm, and the dilution was such that the optical absorbance was around 0.1 at the peak absorption wavelength. As an excitation source laser, a wavelength tunable, continuous wave laser (C-wave, Hübner-Photonics) was used. This laser provides laser light in the wavelength range from 450 nm to 650 nm, with a gap between 520 and 540 nm. Afterwards, the excitation beam passes through an optical fiber, which ensures that possible spatial displacement upon varying the excitation wavelength does not affect the measurement. The beam is further guided through a polarizer, attenuator and mechanical chopper operating set to a 6.2 Hz chopping frequency before being focused onto the cuvette by two convex lenses. A 633 nm HeNe-laser, serving as probe laser, is parallelized ($< 1$ mm apart) to the pump beam via a beam splitter. The deflection of the probe beam is turned into a voltage by a position-sensitive detector, measured by an SR830 lock-in amplifier at a chopping frequency of 6.2 Hz. The luminescent light is captured by two convex lenses and focused onto a silicon photodetector. Before reaching the photodetector, the light is passed through an optical filter, blocking out the excitation laser source beam. The subsequent current produced by the photodetector is quantified by a second SR830 lock-in amplifier. Finally, a third SR830 lock-in amplifier is used to record the intensity of the pump beam, which is measured by a pyro-electric detector. In conjunction, the photoluminescence spectrum is measured by focusing the luminescent emission with two lenses on an Andor Kymera 328i spectrograph with an iDus 416 CCD camera. The lens/spectrometer system is calibrated by using a halogen calibration lamp (Avantes) with known intensity.
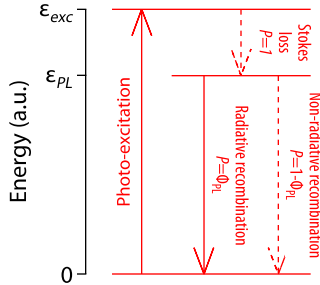
Figure 2: Energetic transitions relevant for the concept of the photothermal threshold quantum yield method, including the ($\varepsilon_{exc}$) the energy absorbed upon photo-excitation of a luminophore, ($\varepsilon_{exc} - \varepsilon_{PL}$) the Stokes loss involved in relaxation of the photo-excited state, and ($\varepsilon_{PL}$) the energy involved in recombination of the relaxed photo-excited state. Transitions involving thermal dissipation are indicated through dashed arrows, while $P$ indicates the probability for each transition to occur.

# The Photothermal Threshold Quantum Yield Method

## The Measurement Concept

As outlined schematically in **Figure 2**, photon absorption by a luminophore either results in photon emission or the generation of thermal energy. The photoluminescence quantum yield $\Phi_{PL}$ expresses the probability for energy conversion via photon emission, and the emission spectrum provides the breakdown of this probability across a set of energy ranges. As such, the emission spectrum can be used to calculate the average energy of the photoluminescent photons, a quantity we will refer to as the average photoluminescence energy $\varepsilon_{PL}$. For the conversion of the absorbed photon energy to thermal energy, a further subdivision must be made:

1. *Stokes losses*. Thermal energy dissipated by the relaxation of photo-excited charge carriers to the excited state from which, subsequently, emission will occur.

2. *Non-radiative recombination losses.* Thermal energy dissipated by the non-radiative decay of the relaxed photo-excited state.

Importantly, non-radiative recombination losses depend on $\Phi_{PL}$, but are not directly dependent on excitation energy, while the thermal energy generated by the relaxation of the photo-excited

7

state is independent of $\Phi_{\text{PL}}$, yet depends directly on the excitation energy, see Figure 2. This distinction is key to the photothermal threshold quantum yield method, and ultimately enables the PLQY of a luminophore to be precisely determined in the common case that $\Phi_{\text{PL}}$ is excitation energy independent. .

The probability that a relaxed photo-excited state decays through non-radiative recombination is, by definition, $1 - \Phi_{\text{PL}}$. The thermal energy generated by such a non-radiative event is equal to the energy of an emitted photon, which is on average $\varepsilon_{PL}$. Thus, heat is generated by non-radiative recombination of the relaxed photo-excited state at a rate $P_{NR}$ given by:

$$P_{NR} = N_{abs} \times (1 - \Phi_{\text{PL}}) \varepsilon_{PL} \tag{1}$$

Here, $N_{abs}$ is the absorbed photon flux. Similarly, the thermal energy related to Stokes losses after a single excitation equals the difference between the energy $\varepsilon_{exc}$ of the photons used for photo-excitation and the energy $\varepsilon_{PL}$ of the emitted photons. Hence, the heat transfer rate $P_S$ due to Stokes losses amounts to:

$$P_S = N_{abs} \times (\varepsilon_{exc} - \varepsilon_{PL}) \tag{2}$$

Adding both relations, we obtain the total thermal loss rate $P_{TL}$ upon photo-excitation of a given set of luminophores as:

$$P_{TL} = N_{abs} \times (\varepsilon_{exc} - \Phi_{\text{PL}} \varepsilon_{PL}) = N_{abs} \times \varepsilon_{TL} \tag{3}$$

Here, $\varepsilon_{TL}$ is the average thermal energy loss per absorbed photon. Finally, next to the thermal losses, the power $P_{PL}$ emitted through photoluminescence amounts to:

$$P_{PL} = N_{abs} \times \Phi_{\text{PL}} \varepsilon_{PL} \tag{4}$$

What is measured in the PTQY method, is a signal $\mathrm{PLx}(\varepsilon_{exc})$ proportional to $P_{PL}$, and a signal $\mathrm{PDS}(\varepsilon_{exc})$ proportional to the thermal loss $P_{TL}$, which we both wrote explicitly as a function of the excitation energy. As both signals will be proportional to $N_{abs}$, their ratio will be proportional to the average thermal loss $\varepsilon_{TL}$ per absorbed photon:

$$\frac{\mathrm{PDS}}{\mathrm{PLx}} = C \times (\varepsilon_{exc} - \Phi_{\mathrm{PL}}\varepsilon_{PL}) = C \times \varepsilon_{TL} \tag{5}$$

Note that when $\Phi_{\mathrm{PL}}$ is independent of the excitation energy, the constant $C$ will be independent of $\varepsilon_{exc}$ as well. Given this relation, the PTQY method therefore involves the simultaneous measurement of $\mathrm{PDS}(\varepsilon_{exc})$ and $\mathrm{PLx}(\varepsilon_{exc})$, and the analysis of the ratio of both quantities. In case $\Phi_{\mathrm{PL}}$ is independent of the excitation energy, the ratio PDS/PLx will depend linearly on $\varepsilon_{exc}$. Moreover, the extrapolated intercept with the $\varepsilon_{exc}$ axis corresponds to the photothermal threshold energy, $\varepsilon_T = \Phi_{\mathrm{PL}}\varepsilon_{PL}$. A measurement of $\varepsilon_{PL}$ with a well-calibrated spectrometer thus yields $\Phi_{\mathrm{PL,PT}}$, i.e., the PLQY as measured using photothermal quantum yield measurements.

## The Measurement Setup

As shown in **Figure 3a** and **Supporting Information S3**, we implemented a PTQY setup in which a liquid solution of luminophores, such as an organic dye or QDs, is exposed to chopped light from a wavelength-tunable CW laser, which serves as the excitation beam. Part of the photoluminescent photons emitted by the luminophores are detected by an intensity detector. Scanning across a range of excitation wavelengths and recording the intensity detector's signal yields the signal $\mathrm{PLx}(\varepsilon_{exc})$. Simultaneously, a photo-thermal deflection spectroscopy (PDS) configuration is used to measure the relative amount of heat generated in the solution, which corresponds to the signal $\mathrm{PDS}(\varepsilon_{exc})$. For this measurement, a steady-state probe laser beam is aligned parallel with the excitation beam. The absorption of the chopped excitation laser induces a periodic temperature gradient in the cuvette. Since the refractive
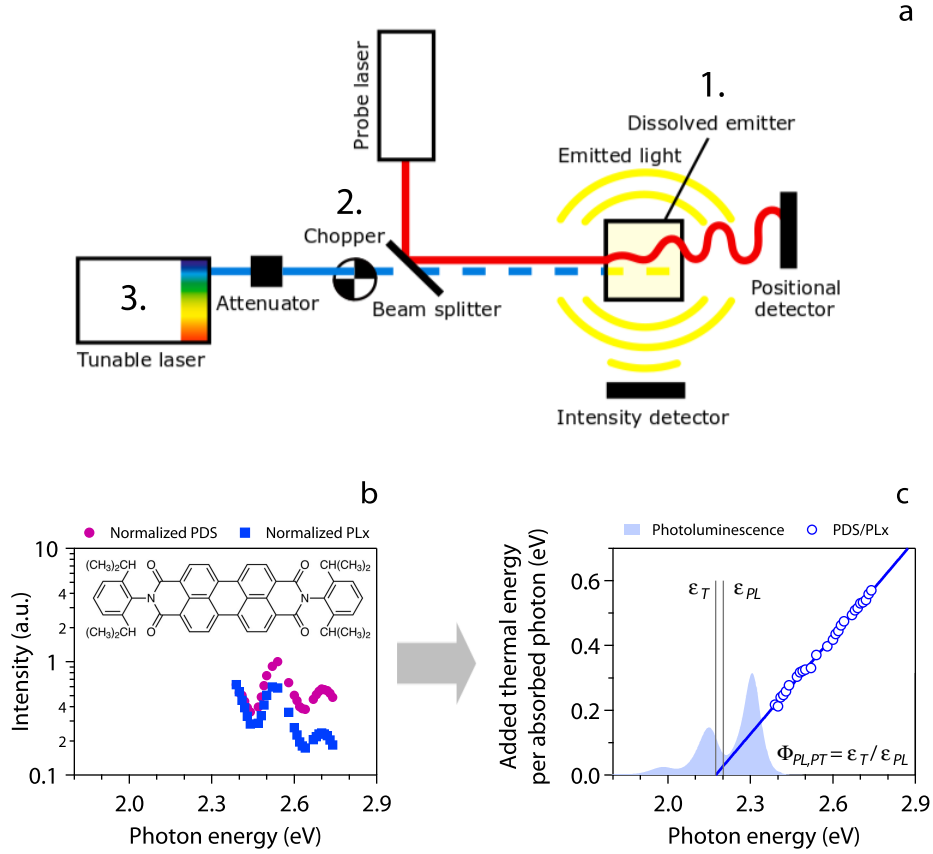
Figure 3: (a) Illustration of the setup used for the PTQY-method. (b,c) Illustration of the measurement protocol, outputted data, and the ensuing data analysis using data recorded on perylene orange as depicted in the inset of (b). The purple disks and blue squares are the normalized photothermal deflection spectrum (PDS) and photoluminescence excitation spectrum (PLx), respectively. The blue circles indicate the PDS/PLx ratio, which we rescaled to yield the thermal loss per absorbed photon. The blue line is the linear regression fit to PDS/PLx. The shaded blue area displays the photoluminescence spectrum. The extrapolated photothermal threshold energy $\varepsilon_T$ and central photon energy of the PL spectrum $\varepsilon_{PL}$ are marked by vertical lines. The photothermal threshold quantum yield $\Phi_{\mathrm{PLPL,PT}}$ is finally determined as $\dfrac{\varepsilon_T}{\varepsilon_{PL}}$.

index of the liquid is temperature-dependent, the probe beam passes through a refractive index gradient, by which the beam deflects through thermal lensing. This periodic deflection is measured by a position-sensitive detector coupled to a lock-in amplifier. At low excitation intensities, the PDS signal is proportional to the rate of heat dissipation by the sample.[36] To ensure that the PDS signals remain in the linear regime, a PID-controlled attenuator is placed in between the tunable CW excitation source and the sample.

## The Measurement Protocol

For a PTQY measurement, we used the protocol outlined in the Materials and Methods section. This protocol can be broken down in different steps:

1. Place the cuvette containing the QD dispersion at a predetermined position in the setup where both pump and probe beam are aligned in parallel (see position 1 in **Figure 3a**).

2. Set the optical chopper to 6.2 Hz (see position 2 in **Figure 3a**) and select appropriate PID-values for controlling the attenuator. The attenuator adjusts the intensity of the pump beam that is incident on the sample such that the generated heat (PDS-signal) remains constant over time and for all excitation photon energies, and should be set so as to operate within a linear deflection regime.

3. Scan the pump laser (see position 3 in **Figure 3a**) across a predetermined set of excitation photon energies, starting with the lowest energy. Allow the system to settle for 30 s each time the pump laser reaches a desired excitation photon energy.

4. Per excitation photon energy, record 30 data points from the three lock-in amplifiers (pump beam intensity, PLx and PDS, all set to a time constant of 1 s) recorded at intervals of 10 s. Data selection and data averaging is discussed in more detail in **Supporting Information S3**. An example of such PLx and PDS curves recorded on perylene orange is provided in **Figure 3b**.[33]

5. Discard a measurement point for which the pump laser/attenuator did not reach the predetermined constant value for the PDS-signal, e.g., due to insufficient or excessive pump laser power.

6. Rerun the entire measurement after scanning the entire range of excitation photon energies.

Through this protocol, a full measurement comprises at least two scans, where a scan consists of measurements for all preset excitation photon energies, delivered by the tunable laser. In

general, such a scan takes several hours, yet recording at least two scans is important. As illustrated in **Supporting Information S4**, the occurrence of photodegradation during a PTQY measurement can be inferred from the systematic decrease of the PLx signal intensity throughout consecutive scans at a given excitation energy of the pump. In case significant photo-degradation occurs, the measurement is to be repeated on a fresh sample with a significantly shorter scan time, for example by using less excitation energies. Such an adaptation of the measurement protocol will, unavoidably, lower the accuracy of the eventually quantum yield estimate.

## Data Analysis and Error Estimation

According to the implemented protocol, a single data point is directly recorded from a lock-in amplifier, and consists of both the amplitude and phase of the measured signal, making up a vector. As detailed in **Supporting Information S3**, the vectors representing the corresponding measurement points are averaged for each excitation energy $\varepsilon_{exc}$ and each lock-in amplifier. For each of the measured signals, the amplitude of the resulting vector then yields either $\mathrm{PDS}(\varepsilon_{exc})$, $\mathrm{PLx}(\varepsilon_{exc})$ or the pump beam intensity. Next, the ratio $\mathrm{PDS}(\varepsilon_{exc})/\mathrm{PLx}(\varepsilon_{exc})$ is determined and plotted as a function of $\varepsilon_{exc}$, see **Figure 3c**. As outlined previously, this quantity is proportional to the total thermal energy $\varepsilon_{TL}$ per absorbed photon added to the sample by the pump beam. Provided that $\Phi_{\mathrm{PL}}$ is excitation-energy independent, $\varepsilon_{TL}$ depends linearly on the excitation energy. Therefore, $\varepsilon_{TL}$ is fitted by simple linear regression to obtain a slope $a$ and an $y$-intercept $b$, as illustrated in **Figure 3c**. Note that the data can be rescaled so as to yield $a = 1$ without affecting the eventual determination of $\Phi_{\mathrm{PL,PT}}$

For $n$ different $(\varepsilon_{exc}, \varepsilon_{TL})$ data couples, the best fit for $a$ and $b$ is obtained by the following

equations:

$$a = \frac{n \sum_{i=1}^{n} \varepsilon_{exc,i} \varepsilon_{TL,i} - \sum_{i=1}^{n} \varepsilon_{exc,i} \sum_{i=1}^{n} \varepsilon_{TL,i}}{n \sum_{i=1}^{n} \varepsilon_{exc,i}^2 - (\sum_{i=1}^{n} \varepsilon_{exc,i})^2} \tag{6}$$

$$b = \frac{1}{n} \sum_{i=1}^{n} \varepsilon_{TL,i} - \frac{a}{n} \sum_{i=1}^{n} \varepsilon_{exc,i} \tag{7}$$

Furthermore, the standard deviation on $a$ and $b$ is calculated as:

$$s_a^2 = \frac{n \sum_{i=1}^{n} \varepsilon_{TL,i} - (\sum_{i=1}^{n} \varepsilon_{TL,i})^2 - a^2(n \sum_{i=1}^{n} \varepsilon_{exc,i}^2 - (\sum_{i=1}^{n} \varepsilon_{exc,i})^2)}{(n-2)(\sum_{i=1}^{n} \varepsilon_{exc,i}^2 - (\sum_{i=1}^{n} \varepsilon_{exc,i}^2))} \tag{8}$$

$$s_b^2 = \frac{s_a^2}{n} \sum_{i=1}^{n} E_i^2 \tag{9}$$

Finally, the following equations define a 95% confidence region:

$$a \in [a \pm t_n^* s_a] \tag{10}$$

$$b \in [b \pm t_n^* s_b] \tag{11}$$

Here, $t_n^*$ is the 0.975 quantile of Student's t-distribution with $n$ degrees of freedom.

Using the results of the linear regression, the photothermal threshold energy $\varepsilon_T$ is obtained as $-b/a$, whereas the $y$-intercepts of the 95% confidence region determine the confidence intervals for $\varepsilon_T$. Next, the average emission energy $\varepsilon_{PL}$ is calculated by directly averaging the emission spectrum: $I_{PL}(\varepsilon)$ according to:

$$\varepsilon_{PL} = \frac{\int_0^\infty I_{PL}(\varepsilon)\varepsilon d\varepsilon}{\int_0^\infty I_{PL}(\varepsilon)d\varepsilon} \tag{12}$$

Eventually, the photoluminescence quantum yield is calculated as $\Phi_{\text{PL,PT}}$:

$$\Phi_{\text{PL,PT}} = -\frac{b}{a}\frac{1}{\varepsilon_{PL}} = \frac{\varepsilon_T}{\varepsilon_{PL}} \tag{13}$$

For the example of perylene orange as depicted in **Figure 3c**, we thus obtain $\Phi_{\text{PL,PT}} = 98.7\%$.

13

# Impact of an Excitation-Dependent Photoluminescent Quantum Yield

As outlined before, the PTQY method analyses the ratio between $\text{PDS}(\varepsilon_{exc})$ and $\text{PLx}(\varepsilon_{exc})$, which is proportional to the energy $\varepsilon_{TL}$ dissipated per absorbed photon. As both quantities depend on $\Phi_{\text{PL}}$, the linear relation between $\varepsilon_{TL}$ and $\varepsilon_{exc}$ may be compromised if $\Phi_{\text{PL}}$ changes with $\varepsilon_{exc}$. To assess the impact of a variation of an excitation-energy dependent PLQY, we write $\Phi_{\text{PL}}$ as:

$$\Phi_{\text{PL}} = \Phi_{\text{PL},0} + \frac{d\Phi_{\text{PL}}}{d\varepsilon_{exc}}\left(\varepsilon_{exc} - \varepsilon_{PL}\right) \tag{14}$$

Here, $\Phi_{\text{PL},0}$ is the PLQY for an excitation energy equal to $\varepsilon_{PL}$. Using this relation, one can readily write down the following approximate relation for $\text{PDS}(\varepsilon_{exc})/\text{PLx}(\varepsilon_{exc})$:

$$\frac{\text{PDS}(\varepsilon_{exc})}{\text{PLx}(\varepsilon_{exc})} \propto \varepsilon_{exc} - \Phi_{\text{PL},0}\varepsilon_{PL} - \frac{1}{\Phi_{\text{PL},0}}\frac{d\Phi_{\text{PL}}}{d\varepsilon_{exc}}\varepsilon_{exc}\left(\varepsilon_{exc} - \varepsilon_{PL}\right) \tag{15}$$

**Figure 4a-b** represent such simulated heat-per-excitation traces for the case where $\Phi_{\text{PL},0}$ is either 0.95 or 0.80. One sees that in the depicted case, where $\Phi_{\text{PL}}$ goes down with excitation energy, the additional heat released at increasing $\varepsilon_{exc}$ raises the trace as compared to the case of a constant PLQY. Moreover, the different slope at around $\varepsilon_{exc} = \varepsilon_{PL}$ will lead to extrapolation errors that result in an overestimation of $\Phi_{\text{PL}}$. More precisely, the extrapolated intersect will be given by:

$$\Phi_{\text{PL},\text{PT}} = \frac{\Phi_{\text{PL},0} - \frac{1}{\Phi_{\text{PL},0}}\frac{d\Phi_{\text{PL}}}{d\varepsilon_{exc}}\varepsilon_{PL}}{1 - \frac{1}{\Phi_{\text{PL},0}}\frac{d\Phi_{\text{PL}}}{d\varepsilon_{exc}}\varepsilon_{PL}} \tag{16}$$

As can be seen in **Figure 4c**, the impact is more significant the smaller $\Phi_{\text{PL},0}$ and the larger $d\Phi_{\text{PL}}/d\varepsilon_{exc}$. On the other hand, one also sees that such conditions lead to a more significant deviation of the heat-per-excitation curve from linearity. Analysing heat-per-excitation curves for linearity is therefore an essential step in a PTQY analysis.
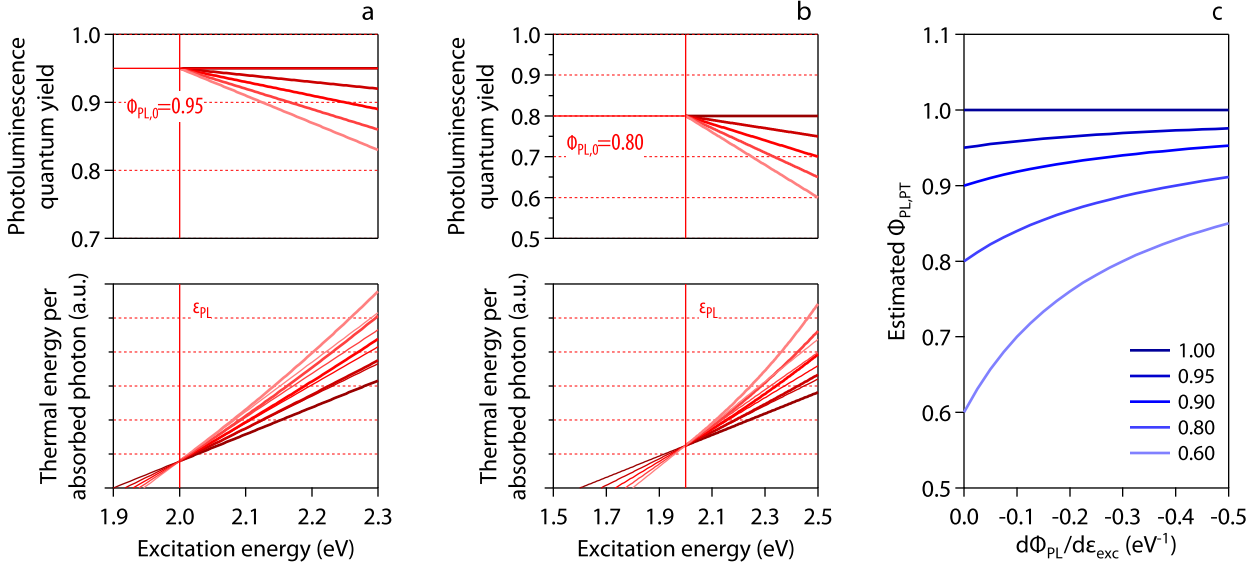
Figure 4: Illustration of the impact of an excitation-energy dependence of the PLQY. (a) (bottom) Heat-per-excitation curves in agreement with the variation of $\Phi_{\mathrm{PL}}$ with excitation energy as indicated in the top graph for the case that $\Phi_{\mathrm{PL}} = 0.95$ for resonant excitation at $\varepsilon_{exc} = \varepsilon_{PL}$. Thin lines represent the linear extrapolation of the heat-per-excitation curves around $\varepsilon_{exc} = \varepsilon_{PL}$. (b) The same for $\Phi_{\mathrm{PL}} = 0.80$. (c) Estimated $\Phi_{\mathrm{PL,PT}}$ using a linear extrapolation around $\varepsilon_{exc} = \varepsilon_{PL}$ as a function of the slope $d\Phi_{\mathrm{PL}}/d\varepsilon_{exc}$ for different values of $\Phi_{\mathrm{PL},0}$ as indicated.

## Limitations and Pittfalls

While the PTQY method can achieve high precision, it has some limitations and pitfalls:

1. A measurement takes in general several hours, exceeding the measurement time of an integrating-sphere measurement. The reason for the larger measurement time is twofold:

   (a) Switching to another excitation wavelength can take up to 10 minutes using the currently available tunable CW laser sources. This time requirement is a purely technical constraint required to obtain a stable laser output.

   (b) Irrespective of the switching time of the tunable laser, a measurement point takes approximately 5 minutes to ensure a sufficient measurement precision.

   The number of measurement points can be minimized, at the cost of precision, yet such

15

a minimal measurement will still take about 1 hour. During this time, the sample is subject to the optical power of the pump laser. Samples prone to photo-degradation are therefore more difficult to analyze using the PTQY method. It should be noted that photo-degradation during the measurement can be detected by comparing the PLQY obtained from successive scans.

2. The PTQY method is most precise for high PLQY-materials. Upon analyzing a luminophore with a lower PLQY, more heat is generated due to non-radiative recombination, while the heat generated due to thermalization remains the same. As a result, a more extensive extrapolation of the measured data is required to obtain the threshold energy $\varepsilon_T$, which comes with a larger error on the estimated value.

3. While the integrating sphere method only requires one excitation energy, the PTQY method requires different excitation energies.

4. As outlined in the previous section, for the PTQY method to work, the $\Phi_{\mathrm{PL}}$ should be constant, independent of the excitation photon energy, the excitation photon flux or the absorbed power. As outlined above, a variation of $\Phi_{\mathrm{PL}}$ with $\varepsilon_{exc}$ will mostly lead to non-linear heat-per-excitation curves, even if specific $\Phi_{\mathrm{PL}}(\varepsilon_{exc})$ dependencies could reproduce a linear heat-per-excitation trace. In either case, the deviation between $\Phi_{\mathrm{PLPT}}$ and the actual $\Phi_{\mathrm{PL}}$ will be larger for a lower PLQY. On the other hand, when the PLQY would depend on the absorbed power, a bump in the $\varepsilon_{TL}$ vs. $\varepsilon_{exc}$ curve would be obtained at the absorption peak.
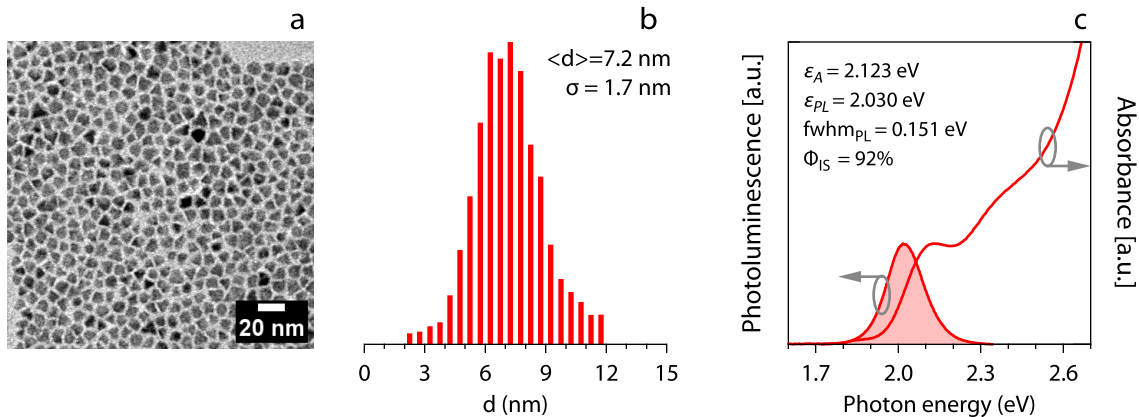
Figure 5: Material characteristics of InP/ZnSe/ZnS QDs (sample A). (a-b) TEM micrograph together with histogram analysis. (c) (red filled curve) Photoluminescence and (red solid curve) UV-VIS absorbance spectrum.

# Photothermal Threshold Quantum Yield of InP/ZnSe/ZnS Quantum Dots

## Material Characteristics

To evaluate and illustrate the PTQY method for the analysis of the PLQY of QD dispersions, we made use of InP/ZnSe/ZnS QDs synthesized with near-unity PLQY using a published protocol that is detailed in **Supporting Information S1**. **Figure 5a** depicts a transmission electron micrograph (TEM) of the sample A InP/ZnSe/ZnS QDs used in this study. In line with previous work, the aminophosphine route yields compact, faceted InP-based core/shell nanocrystals which rather irregular shapes.[18] From the histogram of sizes made from such TEM images, we obtain an average projected diameter $d$ of 7.2 nm and a size dispersion of 1.7 nm, see **Figure 5b**. Absorbance and photoluminescence spectra of the InP/ZnSe/ZnS QDs are presented in **Figure 5c**. The band-edge transition is retrieved at 2.12 eV, while the PL has a maximum intensity at 2.03 eV. On par with the state of the art, the PL spectrum has a full width at half-maximum (fwhm) of 158 meV, and an absolute PLQY ($\Phi_{\mathrm{PL,IS}}$) of 92%, as determined using an integrating sphere.[18] The corresponding metrics for the other

Table 1: Summary of the photothermal quantum efficiency measurements of (first and second column) the different InP-based QDs, including ($\varepsilon_{PL}$) the central photon energy of the PL spectrum, photoluminescence position, ($\varepsilon_T$) the extrapolated threshold energy, ($\Phi_{\text{PL,PT}}$) the PLQY obtained through PTQY, and ($\Phi_{\text{PL,IS}}$) the absolute PLQY obtained by means of an integrating sphere.

| Label | System | $\varepsilon_{PL}$ [eV] | $\varepsilon_T$ [eV] | $\Phi_{\text{PL,PT}}$ [%] | $\Phi_{\text{PL,IS}}$ [%] |
|-------|--------|-------------------------|----------------------|---------------------------|---------------------------|
| A | InP/ZnSe/ZnS | 2.030 | 1.913 | $94.2 \pm 0.3$ | 92 |
| B | InP/ZnSe/ZnS | 2.027 | 1.931 | $95.0 \pm 1.0$ | 99 |
| C | InP/ZnSe/ZnS | 2.032 | 1.934 | $95.0 \pm 1.0$ | 97 |
| D | InP/ZnSe/ZnS | 2.094 | 1.880 | $90.0 \pm 1.0$ | 96 |
| E | InP/ZnSe | 2.038 | 1.070 | $53.0 \pm 5.0$ | 61 |
| F | InP/ZnSe | 2.038 | 1.709 | $84.0 \pm 2.0$ | 83 |

samples are summarized in Table 1, and data overview figures are provided in **Supporting Information Section S5**.

## Photothermal Threshold Quantum Yield of InP-based QD Sols

We determined $\Phi_{\text{PL,PT}}$ of the different batches of InP/ZnSe and InP/ZnSe/ZnS core/shell QD sols using the outlined PTQY protocol. As discussed, a QD dispersion was excited with monochromatic excitation light using a tunable CW laser. The intensity of light emitted by the QDs (PLx) was recorded at each excitation wavelength, in conjunction with the heat produced (PDS), and the relative heat-per-excitation trace was obtained from the ratio of both signals. Using this trace, we determined the zero-loss threshold $\varepsilon_T$ as the intercept between the extrapolated heat-per-excitation trace and the excitation photon energy axis. The ratio between $\varepsilon_T$ and the average photon energy $\varepsilon_{PL}$ of the PL spectrum then yields $\Phi_{\text{PL,PT}}$, i.e., the PLQY determined through PTQY. Note that for all examples shown, $\Phi_{\text{PL,PT}}$ was obtained on samples shipped between two laboratories, while the absolute quantum yield $\Phi_{\text{PL,IS}}$ measured using an integrating sphere was determined prior to the sample transfer.
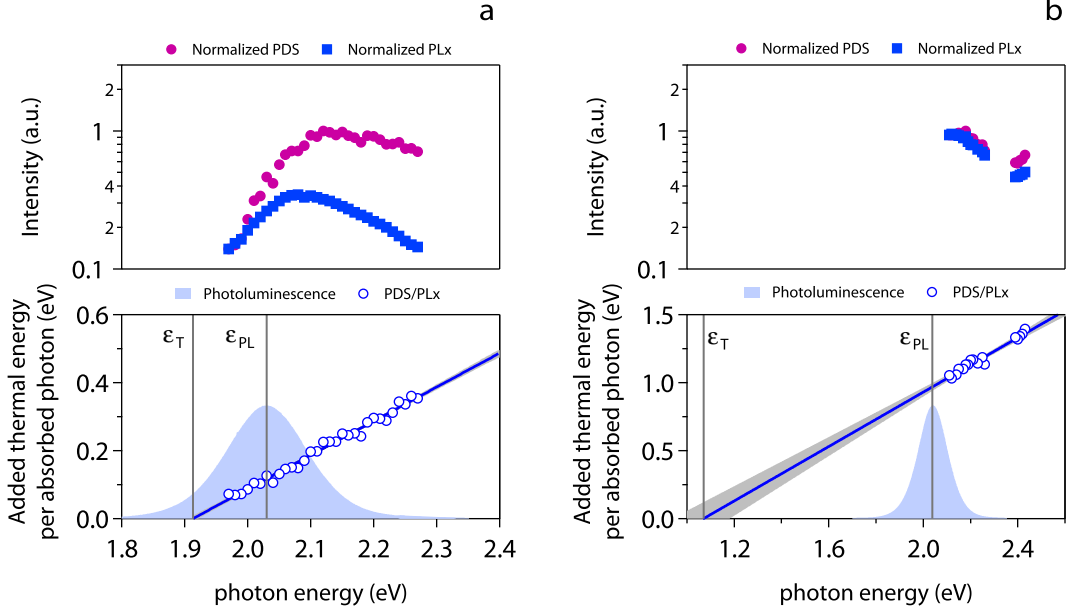
Figure 6: Comparison between (a) near-unity emitting InP/ZnSe/ZnS QDs (sample A), and (b) a reference measurement on InP/ZnSe QDs with a lower PLQY (sample E). (top) The purple disks and blue squares are the normalized PDS and PLx, respectively. (bottom) The PDS/PLx ratio is shown by blue circles. The blue line is the linear regression fit to PDS/PLx, while the filled grey area represents the 95% confidence interval. The shaded blue area is the photoluminescence spectrum. The extrapolated photothermal threshold energy $\varepsilon_T$ and central photon energy of the PL spectrum $\varepsilon_{PL}$ are marked by vertical lines.

**Figure 6a** displays the PL excitation and photothermal deflection signals as recorded on the high-efficiency InP/ZnSe/ZnS QD sample A, in combination with the heat-per-excitation trace that is the ratio of both signals at each excitation photon energy. The heat-per-excitation trace exhibits a clear linear increase as a function of the photon energy, which reflects the additional Stokes losses. For this example, extrapolating the heat-per-excitation trace to obtain the zero-loss threshold yielded $\Phi_{\mathrm{PL,PT}} = 94.2 \pm 0.3\%$. Here, the error reflects a 95% confidence interval. Within the margin of error, this result agrees with $\Phi_{\mathrm{PL,IS}}$, which was determined at $92 \pm 5.0\%$ for the given sample. This agreement indicates that PTQY can be used to obtain the PLQY of QD sols.

To further illustrate the potential of PTQY, **Figure 6b** depicts results of a similar measurement obtained on the InP/ZnSe QD sample E, for which we determined $\Phi_{\mathrm{PL,IS}}$ at 61%. Consistent with the presumed lower PLQY, we find that the heat per excitation

19

measured on this sample for the given analysis settings is significantly higher at equivalent photon energies than for sample A. In line with this observation, extrapolating to $\varepsilon_T$ yields $\Phi_{\text{PL,PT}} = 53.0 \pm 5.0$. As indicated in **Figure 6b**, the larger error in this case is related to the increased uncertainty on the extrapolation of the heat-per-excitation trace. Even so, this margin of error is comparable to that of a single quantum yield measurement by means of an integrating sphere.

We extended the analysis to four more samples, including three InP/ZnSe/ZnS QDs for which we measured a $\Phi_{\text{PL,IS}}$ of 95% or higher, and one InP/ZnSe sample with a lower $\Phi_{\text{PL,IS}}$ of 82%. The recorded PL excitation and photothermal deflection signals, and the resulting heat-per-excitation traces for these different samples can be found in **Supporting Information Section S6**, while **Table 1** provides a summary of the results. As can be seen, the quantum efficiencies determined using an integrating sphere and those recorded through PTQY agree in all cases within the margin of error, despite samples being shipped between two labs for absolute PLQY and PTQY measurements.

## Discussion

Using measurements on InP-based core/shell QDs, we illustrated how PTQY measurements can be used to determine the PLQY of a batch of dispersed QDs, for which we obtained results in agreement with the determination of the PLQY using an integrating sphere. However, as compared to this widely used approach, the PTQY method has significant advantages:

- *Transparency.* The heat-per-excitation curve that results from a PTQY measurement makes for a dataset that can be readily shared as part of a publication or a data sheet.

- *Quality control.* A heat-per-excitation curve mirrors measurement quality. Deviations from linearity, excessive data noise or a too narrow excitation range in relation to the extrapolation all help identifying problematic measurements.

20

- *Precision.* The multiple measurements constituting the heat-per-excitation curve lead to a highly precise estimate of the photothermal threshold, and help identifying potential degradation during the measurement. As illustrated in this work, precision in the case of QD samples can be as low as 0.3%, a stark contrast with a single shot integrating-sphere measurement.

- *Accuracy.* Recording PDS and PLx, and determining $\Phi_{\mathrm{PL,PT}}$ from the heat-per-excitation curve does not require measurements on blank samples. The measurement accuracy depends solely on the intensity and wavelength calibration of the spectrometer used to determine the average emission energy, which strongly reduces errors related to measurement procedures.

Given its providing a verifiable and precise determination of $\Phi_{\mathrm{PL}}$, PTQY measurements could be a method of choice for the certification of the PLQY of a given QD batch, or the average PLQY of QDs obtained through a given synthetic protocol. Using PTQY for PLQY certification is especially relevant since the method is most precise for samples with near-unity PLQY, which are the measurements most in need of a verifiable and precise determination of $\Phi_{\mathrm{PL}}$. Opposite from integrating-sphere measurement, however, PTQY is not a commercially available method. In this respect, calibrating or certifying integrating-sphere protocols by means of PTQY measurements could be a first step to enhance the precision of the PLQY reported for QD batches in literature.

## Conclusion

Precise, accurate and verifiable methods to measure the photoluminescence quantum yield of luminophores are essential for research and development involving luminescent materials. This point holds true in particular for research on colloidal QDs, since devices involving QD photoluminescence need a near-unity photoluminescence quantum yield for optimal performance. Here, we outlined a measurement protocol for measuring $\Phi_{\mathrm{PL}}$ in which the

photothermal threshold quantum yield method is applied to QD sols, a state of QD processing that is closest to the as-synthesized QD product. Using the example of InP/ZnSe/ZnS core/shell QDs, we show that the method yields more precise estimates of $\Phi_{PL}$ than optical measurements by means of an integrating sphere. Moreover, by relying on the relative measurement of the thermal loss per excitation, calibration errors are minimized and a dataset is obtained deviations from linearity directly point towards experimental issues. We therefore argue that PTQY should be used as a standard technique for quantum yield determination in the field of colloidal QDs, in particular for analyzing samples with near unity PLQY.

# Acknowledgement

# Supporting Information Available

The Supporting Information contains (S1) Experimental Section, (S2) Photoluminescent Quantum Yield Measurement Using an Integrating Sphere, (S4 Examples of Impact of Photodegradation, (S5) Material Characteristics of InP-based Quantum Dots, and (S6) Photothermal Quantum Efficiency Determination.

# References

(1) Kovalenko, M. V.; Manna, L.; Cabot, A.; Hens, Z.; Talapin, D. V.; Kagan, C. R.; Klimov, X. V. I.; Rogach, A. L.; Reiss, P.; Milliron, D. J.; Guyot-sionnnest, P.; Konstantatos, G.; Parak, W. J.; Hyeon, T.; Korgel, B. A. et al. Prospects of Nanoscience with Nanocrystals. *ACS Nano* **2015**, *9*, 1012–1057.

(2) Yuan, M.; Liu, M.; Sargent, E. H. Colloidal Quantum Dot Solids for Solution-Processed Solar Cells. *Nat. Energy* **2016**, *1*.

(3) Georgitzikis, E.; Malinowski, P. E.; Li, Y.; Maes, J.; Hagelsieb, L. M.; Guerrieri, S.; Zeger, H.; Heremans, P.; Cheyns, D. Integration of PbS Quantum Dot Photodiodes on Silicon for NIR Imaging. *IEEE Sens. J.* **2020**, *20*, 6841–6848.

(4) Hong, Q.; Lee, K.-C.; Luo, Z.; Wu, S.-T. High-Efficiency Quantum Dot Remote Phosphor Film. *Appl. Opt.* **2015**, *54*, 4617–4622.

(5) Bang, S. Y.; Suh, Y.-H.; Fan, X.-B.; Shin, D.-W.; Lee, S.; Choi, H. W.; Lee, T. H.; Yang, J.; Zhan, S.; Harden-Chaters, W.; Samarakoon, C.; Occhipinti, L. G.; Han, S. D.; Jung, S.-M.; Kim, J. M. Technology Progress on Quantum Dot Light-Emitting Diodes for Next-Generation Displays. *Nanoscale Horiz.* **2021**, *6*, 68–77.

(6) Shimizu, K. T.; Böhmer, M.; Estrada, D.; Gangwal, S.; Grabowski, S.; Bechtel, H.; Kang, E.; Vampola, K. J.; Chamberlin, D.; Shchekin, O. B.; Bhardwaj, J. Toward Commercial Realization of Quantum Dot Based White Light-Emitting Diodes for General Illumination. *Photon. Res.* **2017**, *5*, A1–A6.

(7) Karadza, B.; Schiettecatte, P.; Van Avermaet, H.; Mingabudinova, L.; Giordano, L.; Respekta, D.; Deng, Y.-H.; Nakonechnyi, I.; De Nolf, K.; Walravens, W.; others Bridging the Green Gap: Monochromatic InP-Based Quantum-Dot-on-Chip LEDs with over 50% Color Conversion Efficiency. *Nano Lett.* **2023**, *23*, 5490–5496.

(8) Meinardi, F.; Colombo, A.; Velizhanin, K. A.; Simonutti, R.; Lorenzon, M.; Beverina, L.; Viswanatha, R.; Klimov, V. I.; Brovelli, S. Large-Area Luminescent Solar Concentrators based on 'Stokes-Shift-Engineered' Nanocrystals in a Mass-Polymerized PMMA Matrix. *Nat. Phot.* **2014**, *8*, 392–399.

(9) Krumer, Z.; Pera, S. J.; van Dijk-Moes, R. J. A.; Zhao, Y.; de Brouwer, A. F. P.; Groeneveld, E.; van Sark, W. G. J. H. M.; Schropp, R. E. I.; Donega, C. d. M. Tackling Self-Absorption in Luminescent Solar Concentrators with Type-II Colloidal Quantum Dots. *Sol. Energy Mater. Sol. Cells* **2013**, *111*, 57–65.

(10) Houtepen, A. J.; Hens, Z.; Owen, J. S.; Infante, I. On the Origin of Surface Traps in Colloidal II–VI Semiconductor Nanocrystals. *Chem. Mater.* **2017**, *29*, 752–761.

(11) Hines, M. A.; Guyot-Sionnest, P. Synthesis and Characterization of Strongly Luminescing ZnS-Capped CdSe Nanocrystals. *J. Phys. Chem.* **1996**, *100*, 468–471.

(12) Donega, C. d. M. Synthesis and Properties of Colloidal Heteronanocrystals. *Chem. Soc. Rev.* **2011**, *40*, 1512–1546.

(13) Jang, Y.; Shapiro, A.; Isarov, M.; Rubin-Brusilovski, A.; Safran, A.; Budniak, A. K.; Horani, F.; Dehnel, J.; Sashchiuk, A.; Lifshitz, E. Interface Control of Electronic and Optical Properties in IV-VI and II-VI Core/Shell Colloidal Quantum Dots: a Review. *Chem. Comm.* **2017**, *53*, 1002–1024.

(14) Kirkwood, N.; Monchen, J. O. V.; Crisp, R. W.; Grimaldi, G.; Bergstein, H. A. C.; du Fosse, I.; van der Stam, W.; Infante, I.; Houtepen, A. J. Finding and Fixing Traps in II-VI and III-V Colloidal Quantum Dots: The Importance of Z-Type Ligand Passivation. *J. Am. Chem. Soc.* **2018**, *140*, 15712–15723.

(15) Mondal, N.; De, A.; Samanta, A. Achieving Near-Unity Photoluminescence Efficiency for Blue-Violet-Emitting Perovskite Nanocrystals. *ACS Energy Lett.* **2019**, *4*, 32–39.

(16) Chen, O.; Zhao, J.; Chauhan, V. P.; Cui, J.; Wong, C.; Harris, D. K.; Wei, H.; Han, H.-S.; Fukumura, D.; Jain, R. K.; Bawendi, M. G. Compact High-Quality CdSe-CdS Core-Shell Nanocrystals with Narrow Emission Linewidths and Suppressed Blinking. *Nat. Mater.* **2013**, *12*, 445–451.

(17) Won, Y.-H.; Cho, O.; Kim, T.; Chung, D.-Y.; Kim, T.; Chung, H.; Jang, H.; Lee, J.; Kim, D.; Jang, E. Highly Efficient and Stable InP/ZnSe/ZnS Quantum Dot Light-Emitting Diodes. *Nature* **2019**, *575*, 634–638.

(18) Van Avermaet, H.; Schiettecatte, P.; Hinz, S.; Giordano, L.; Ferrari, F.; Nayral, C.; Delpech, F.; Maultzsch, J.; Lange, H.; Hens, Z. Full-Spectrum InP-Based Quantum Dots with Near-Unity Photoluminescence Quantum Efficiency. *ACS Nano* **2022**,

(19) Li, Y.; Hou, X.; Dai, X.; Yao, Z.; Lv, L.; Jin, Y.; Peng, X. Stoichiometry-Controlled InP-Based Quantum Dots: Synthesis, Photoluminescence, and Electroluminescence. *J. Am. Chem. Soc.* **2019**, *141*, 6448–6452.

(20) Chae, H.; Jiang, W. Efficiency Enhancement of Tris(dimethylamino)-Phosphine-Based Red Indium Phosphide Quantum-Dot Light-Emitting Diodes via Chlorine-Doped ZnMgO Electron Transport Layers. *J. Phys. Chem. C* **2020**, *124*, 25221–25228.

(21) Liu, P.; Lou, Y.; Ding, S.; Zhang, W.; Wu, Z.; Yang, H.; Xu, B.; Wang, K.; Sun, X. W. Green InP/ZnSeS/ZnS Core Multi-Shelled Quantum Dots Synthesized with Aminophosphine for Effective Display Applications. *Adv. Funct. Mater.* **2021**, *31*, 1–7.

(22) Jo, J. H.; Jo, D. Y.; Choi, S. W.; Lee, S. H.; Kim, H. M.; Yoon, S. Y.; Kim, Y.; Han, J. N.; Yang, H. Highly Bright, Narrow Emissivity of InP Quantum Dots Synthesized by Aminophosphine: Effects of Double Shelling Scheme and Ga Treatment. *Adv. Opt. Mater.* **2021**, *2100427*, 1–9.

(23) Yu, P.; Shan, Y.; Cao, S.; Hu, Y.; Li, Q.; Zeng, R.; Zou, B.; Wang, Y.; Zhao, J.

Inorganic Solid Phosphorus Precursor of Sodium Phosphaethynolate for Synthesis of Highly Luminescent InP-Based Quantum Dots. *ACS Energy Lett.* **2021**, *6*, 2697–2703.

(24) Choi, S.-W.; Kim, H.-M.; Yoon, S.-Y.; Jo, D.-Y.; Kim, S.-K.; Kim, Y.; Park, S. M.; Lee, Y.-J.; Yang, H. Aminophosphine-derived, high-quality red-emissive InP quantum dots by the use of an unconventional in halide. *J. Mater. Chem. C* **2022**, *10*, 2213–2222.

(25) Schiettecatte, P.; Giordano, L.; Cruyssaert, B.; Bonifas, G.; De Vlamynck, N.; Van Avermaet, H.; Zhao, Q.; Vantomme, A.; Nayral, C.; Delpech, F.; others Enhanced Surface Passivation of InP/ZnSe Quantum Dots by Zinc Acetate Exposure. *Chem. Mater.* **2024**,

(26) de Mello, J. C.; Wittmann, H. F.; Friend, R. H. An Improved Experimental Determination of External Photoluminescence Quantum Efficiency. *Adv. Mater.* **1997**, *9*, 230–232.

(27) Fries, F.; Reineke, S. Statistical Treatment of Photoluminescence Quantum Yield Measurements. *Sci. Rep.* **2019**, *9*, 15638.

(28) Pauli, J.; Güttler, A.; Schneider, T.; Würth, C.; Resch-Genger, U. Fluorescence Quantum Yield Standards for the UV/Visible/NIR: Development, Traceable Characterization, and Certification. *Anal. Chem.* **2023**, *95*, 5671–5677.

(29) Olmsted, J. Calorimetric Determinations of Absolute Fluorescence Quantum Yields. *J. Phys. Chem.* **1979**, *83*, 2581–2584.

(30) Boudebs, G.; Zinoune, J.-B.; Cassagne, C.; Chis, M. Thermal Lens Z-scan Measurements: Theoretical and Experimental Uncertainties for Low and High Fluorescence Quantum Yields. *Appl. Opt.* **2023**, *62*, 7669–7677.

(31) Couch, B.; Meyer, A.; Heller, B.; Johnson, S. L. Absolute Fluorescence Quantum Yield Determined by Photothermal Deflection Spectroscopy. *Methods. Appl. Fluoresc.* **2019**, *7*.

(32) Hanifi, D. A.; Bronstein, N. D.; Koscher, B. A.; Nett, Z.; Swabeck, J. K.; Takano, K.; Schwartzberg, A. M.; Maserati, L.; Vandewal, K.; van de Burgt, Y.; others Redefining Near-Unity Luminescence in Quantum Dots with Photothermal Threshold Quantum Yield. *Science* **2019**, *363*, 1199–1202.

(33) Mertens, S.; Siegmund, B.; Vandewal, K. Ultra-Precise Photothermal Measurements Reveal Near Unity Photoluminescence Quantum Yields of Molecular Emitters in Solution. *Mater. Horiz.* **2023**, *10*, 594–600.

(34) Tessier, M. D.; Dupont, D.; De Nolf, K.; De Roo, J.; Hens, Z. Economic and Size-Tunable Synthesis of InP/ZnE (E = S, Se) Colloidal Quantum Dots. *Chem. Mater.* **2015**, *27*, 4893–4898.

(35) Leyre, S.; Coutino-Gonzalez, E.; Joos, J.; Ryckaert, J.; Meuret, Y.; Poelman, D.; Smet, P.; Durinck, G.; Hofkens, J.; Deconinck, G.; others Absolute Determination of Photoluminescence Quantum Efficiency using an Integrating Sphere Setup. *Rev. Sci. Instrum.* **2014**, *85*.

(36) Boccara, A. C.; Fournier, D.; Jackson, W.; Amer, N. M. Sensitive photothermal deflection technique for measuring absorption in optically thin media. *Opt. Lett.* **1980**, *5*, 377–379.